EUROfusion

EUROFUSION WPJET1–PR(15)30

N. Bonanomi et al.

Trapped Electron Mode Driven Electron Heat Transport in JET: Experimental Investigation and Gyro–Kinetic Theory Validation

Preprint of Paper to be submitted for publication in
Nuclear Fusion

This work has been carried out within the framework of the EUROfusion Consortium and has received funding from the Euratom research and training programme 2014-2018 under grant agreement No 633053. The views and opinions expressed herein do not necessarily reflect those of the European Commission.

Trapped electron mode driven electron heat transport in JET: experimental investigation and gyro-kinetic theory validation.

N. Bonanomi[1,2], P. Mantica[1], G. Szepesi[1,6], N. Hawkes[6], E. Lerche[3], P. Migliano[4], A. Peeters[4], C. Sozzi[1], M. Tsalas[5,6], D. Van Eester[3] and JET Contributors*

EUROfusion Consortium, JET, Culham Science Centre, Abingdon, OX14 3DB, UK

1)Istituto di Fisica del Plasma CNR, Milano, Italy

2)Università degli Studi di Milano-Bicocca, Milano, Italy

3)LPP-ERM/KMS, TEC partner, Brussels, Belgium

4)University of Bayreuth, Germany

5)FOM Institute DIFFER, TEC partner, Nieuwegein, The Netherlands

6)Culham Centre for Fusion Energy, Abingdon, OX14 3DB, UK

Abstract

The main purpose of this work is to study the dependence of Trapped Electron Mode (TEM) threshold and of electron stiffness on the most relevant plasma parameters. Dedicated transport experiments based on heat flux scans and T_e modulation have been performed in JET in TEM dominated plasmas with pure ICRH electron heating and a numerical study using gyrokinetic simulations has been performed with the code GKW. Using multilinear regressions on the experimental data, the stabilizing effects of magnetic shear and collisionality predicted by theory for our plasma parameters are confirmed. Good quantitative agreement is found between the TEM thresholds found in the experiments and calculated with linear GKW simulations. Non-linear simulations have given further confirmation of the threshold values and allowed comparison with the values of stiffness found experimentally. Perturbative studies using RF power modulation indicate the existence of an inward convective term for the electron heat flux. Adding NBI power, Ion Temperature Gradient (ITG) modes become dominant and a reduction of $|\nabla T_e|/T_e$ with respect pure ICRH, TEM dominant discharges has been experimentally observed, in spite of increased total electron power. Possible explanations are discussed.

*See the Appendix of F. Romanelli et al., Proceedings of the 25th IAEA Fusion Energy Conference 2014, Saint Petersburg, Russia

Introduction

Recent findings on JET that ion heat transport can be considerably reduced in the core by electromagnetic effects related to high thermal and supra-thermal pressure gradients [1,2] have opened positive perspectives of reaching improved confinement regimes at high β. However, before extrapolating to ITER from present machines with dominant NBI ion heating, it is essential to complete the understanding of electron heat transport, which in ITER electron heating dominated plasmas may limit the benefits of improved ion confinement.

This paper is part of a long-lasting effort to characterize electron heat transport driven by Trapped Electron Modes (TEMs) by means of dedicated experiments and theoretical modeling. Theory indicates that there is a critical value of the normalized inverse temperature gradient length $R/L_{Te} = R|\nabla T_e|/T_e$ (with R the tokamak major radius) above which TEM modes become unstable [3,4], so electron heat transport features a threshold $(R/L_{Te})_{crit}$, or κ_c, above which the electron heat flux increases strongly with R/L_{Te}. This property leads to stiffness of T_e profiles with respect to changes in heating profiles. The level of stiffness χ_s characterizes how strongly T_e profiles are tied to the threshold.

Numerical studies of TEM linear growth rate and threshold have been performed using linear gyrokinetic simulations with the code GS2 and the code KINEZERO, on the role of plasma parameters such as $s, R/L_n$ and effective collisionality $\nu_{eff} \approx 0.1 \cdot Z_{eff} \cdot n_e \cdot R/T_e^2$ on electron heat transport due to TEMs. These simulations predict a stabilizing effect of the magnetic shear [5] and a dependence of the effect of collisionality on other plasma parameters, in particular on R/L_n [6]. In all the plasmas studied in this paper, the values of the density gradient and of the collisionality are such that a stabilizing effect of collisionality is expected. Experiments done in tokamak ASDEX-Upgrade confirmed the stabilizing effect of collisionality on TEMs in our range of parameters [7], but no experimental evidence of the roles of magnetic shear and of density gradient has been obtained yet. The correlation between TEM threshold and the ratio of electron to ion temperature T_e/T_i has been investigated analytically and with linear gyrokinetic simulations with the code KINEZERO [7]. These studies predict different effects of T_e/T_i on TEM threshold depending on the value of R/L_n: for low values of R/L_n ($R/L_n \lesssim 1.3$) they predict a stabilizing effect of T_e/T_i, while a destabilizing effect of the same parameter is predicted with higher values of R/L_n. Studies on electron stiffness have been done on different machines. Studies performed on tokamak DIII-D indicate that stiffness increases with radius. A higher electron stiffness in presence of NBI heating was also observed in other studies in ASDEX-Upgrade, JET and DIII-D [9, 10, 11].

The aim of this paper is to study the dependence of turbulent electron heat transport due to TEMs on plasma parameters in JET plasmas with dominant RF electron heating obtained by ICRH in Mode Conversion and to compare the experimental observations with theory-based models, with also a comparison to previous studies. In particular, experimentally we identify separately the values of threshold and stiffness, which allows a more stringent comparison with theoretical predictions. Lastly, initial results of an investigation of the effect of the presence of significant ion heating (NBI) on TEMs are presented.

The paper is organized as follows: in section 1 we present the experimental set up; in section 2 the main experimental observations in plasmas with dominant electron heating are presented; in section 3 the modeling effort is described and its results are compared with the experimental observations; in section 4 the effects of the presence of NBI heating are discussed; summary and conclusions are

	78830	**78834**	**78835**	**78836**	**78839**	**78840**	**78842**
B **(T)**	3.45	3.45	3.45	3.45	3.45	3.45	3.45
I_p **(MA)**	1.8 - 3 Ramp-up	1.8 Overshoot	1.8 Overshoot	1.8 Overshoot	3 - 1.8 Ramp-down	3 -1.8 Ramp-down	1.8 Overshoot
$ICRH$ **(MW)**	2.5	3	2.5	3	3	2.5	3
ν_{ICRH} **(MHz)**	32 On-axis	32 On-axis	37 Off-axis	37 Off-axis	32 Off-axis	37 On-axis	37 On-axis
NBI **(MW)**	0	0	0	6.8	0	0	6.8
$T_{e,0}$ **(keV)**	4	4	3	5	4	4	5
$T_{i,0}$ **(keV)**	2.5	2.5	2	5	2.5	2.5	5
$n_{e,0}$ **(m^{-3})**	3	3	3	3	3	3	3
Z_{eff}	2.2	2.2	2.2	2.2	2.2	2.2	2.2

Table 1: *Main parameters of the TEM session discharges.*

presented in section 5.

1 Experimental set up and methods

The discharges studied in this paper were made in the JET tokamak ($R = 2.96$ m $a \approx 1$ m) and are all L-mode ($^3He) - D$ plasmas with $B_T \approx 3.45$ T, $n_{e,0} \approx (2\text{–}3) \cdot 10^{19}$ m^{-3} and $I_p \approx 1.8 - 3$ MA. The session dedicated to TEM study is composed of seven discharges (described in Table 1) with ICRH (Ion Cyclotron Resonance Heating) of about $2.5 - 3$ MW deposited directly on electrons via Mode Conversion (MC) using a ^3He concentration $[^3He] \approx 20\%$, which ensures a dominant electron heating with about 70% of the ICRH power deposited on electrons [12].

The RF power was square wave modulated with a 70/30 duty-cycle, a modulation amplitude of about 70% and a frequency of 20 Hz in order to use perturbative techniques to calculate TEM stiffness and threshold [13, 14]. The RF power deposition in MC scheme is not easily and reliably calculated by RF codes, and is therefore calculated by fitting the profiles of modulation amplitudes and phases of different harmonics using adjustable profiles of heat diffusivity, convection and RF heat deposition using the ASTRA transport code (Automated System for TRansport Analysis [15]). Fitting the highest harmonics, which are less influenced by transport and depend mostly on the power deposition, it is estimated that the uncertainty on such reconstruction of RF deposition is in the order of $\pm 10\%$. ICRH power was deposited both on-axis ($R \approx 3.0$ m) and off-axis ($R \approx 3.4$ m) in order to obtain low and high values of heat flux q_e for the study of the electron heat flux scan versus $R/L_{Te} = R\,|\nabla T_e|\,/T_e$. In two of the analyzed discharges , NBI (Neutral Beam Injection) heating of about 6.8 MW was also used in order to study the effect of the presence of significant ion heating , i.e. of ITG modes, on TEM modes. NBI heating also introduces a high rotation of the plasma and the presence of a fast ion population. The NBI heating power on electrons and ions is calculated with the PENCIL code with an uncertainly of about ± 100 kW. The ohmic power density is calculated using $P_{Ohm} = \eta \cdot j^2$, where η is the resistivity of the plasma and j is the plasma current density reconstructed by the EFIT equilibrium code with the MSE (Motional Stark Effect) constraints. The error on the estimated ohmic power is about 5%. The electron heat flux is calculated in gyro-Bohm units as $q_e = [(P_{e,Ohm} + P_{e,ICRH} + P_{e,NBI} - P_{e,rad} - P_{ei})/S] \cdot (R/T_e) \cdot (R/\rho_s^2 c_s)$, where S is the considered flux surface, $P_{e,rad}$ is the radiated power (negligible within $r/R \approx 0.8$), $c_s = \sqrt{T_e/m_i}$ and $\rho_s = c_s m_i/eB$. Typical error on electron heat flux is about 15% of the total flux. The measurement

of the electron temperature T_e is provided by the ECE (Electron Cyclotron Emission) diagnostic with an error on the measurements of about 5% while the ion temperature T_i and plasma rotation ω_t are measured by the Charge Exchange (CX) diagnostic with an error of about 5% for the ion temperature and of about 8% for the plasma rotation. The charge exchange diagnostic needs NBI heating; for the measurements of the ion temperature in discharges without NBI heating, blips of NBI heating of 1.5 MW and $\Delta t = 0.15$ s are used. n_e is measured by high-resolution Thomson scattering (HRTS) with an uncertainty of about 10%. Radial profiles of the ICRH power density on electrons $P_{e,ICRH}$ and of T_e, T_i, n_e, q, s of discharges n. 78834 (on-axis ICRH, no NBI), n. 78839 (off-axis ICRH, no NBI) and 78842 (on-axis ICRH, 7 MW NBI) are shown in Figure 1 and in Figure 2. The time waveforms of heating power of discharges n. 78834 and n. 78842 are shown in Figure 3 (note the ICRH modulation phase between $t = 5.5$ s and $t = 10$ s). The radial profiles of heating power of discharge n. 78834 are reported in Figure 4.

Values of $R/L_{Ti}, R/L_{Te}$ and R/L_n were obtained by linear best fit of $ln(T_i), ln(T_e)$ and $ln(n_e)$ data after having time averaged the measurements over a time interval in which the plasma conditions are stationary (usually$\Delta t \approx \pm 0.25$ s). The uncertainties on these parameters are then estimated by repeating the same procedure with different time and space intervals and evaluating the deviation in the set of values so obtained. Error bars are typically $\Delta(R/L_{Ti}) \approx \pm 0.3$–$0.6, \Delta(R/L_{Te}) \approx \pm 0.25 - 0.5$ and $\Delta(R/L_n) \approx \pm 0.3 - 0.6$. The spatial derivatives in these parameters are taken with respect to the flux surface label $r = (R_{out} - R_{in})/2$, where R_{out} and R_{in} are the outer and inner boundaries of the flux surface on the magnetic axis plane.

By using different time waveforms of the plasma current (I_p ramp-up, ramp-down and overshoot with $1.8 \lesssim I_p \lesssim 3$ MA, Figure 5), independent variations of the safety factor q and of the magnetic shear $\hat{s}$ (Figure 6) needed for the study of the correlation between these parameters and the TEM threshold were obtained. The safety factor q profiles are reconstructed by MSE with an error of about 20%. The error on the values of the magnetic shear $\hat{s}$ is estimated to be $\Delta s \approx \pm 0.08$. TEM threshold and electron stiffness at a chosen radial location are determined experimentally by quadratic fits on the diagrams of the normalized electron heat flux q_e as a function of R/L_{Te} on data points with $q, s, \nu_{eff}, R/L_n, T_e/T_i$ constant and using the formula (1) given below [16, 17]. Small values of q_e (nearest to threshold) necessary for the fits are obtained near the core ($\rho_{tor} < 0.4$) with off-axis heating while for the study far off-axis ($\rho_{tor} \approx 0.5$) data points from previously existing discharges with ICRH directed on ions are used. The experimental set-up for these discharges is identical to that used for the TEM session except that the ICRH power is directed on ions, for which the power deposition is evaluated with the PION code.

The data analysis is carried out at 3 radial positions, corresponding to normalized radius $\rho_{tor} = \sqrt{(\Phi/\pi B_T)/(\Phi/\pi B_T)_{max}} = 0.33, 0.4, 0.5$, where Φ is the toroidal magnetic flux and B_T is the toroidal magnetic field.

2 TEM studies in dominant electron heating plasmas

The electron heat flux is predicted by theory to follow a gyro-Bohm scaling and to become turbulent above a threshold value of $|\nabla T_e|/T_e$, so that q_e can be written as [16, 17]

$$q_e = q_e^{res} + q^{1.5}\chi_s \frac{n_e T_e^2 \rho_s}{eBR^2} \frac{R}{L_{Te}} \left(\frac{R}{L_{Te}} - \kappa_c\right) \cdot \theta \left(\frac{R}{L_{Te}} - \kappa_c\right) \tag{1}$$

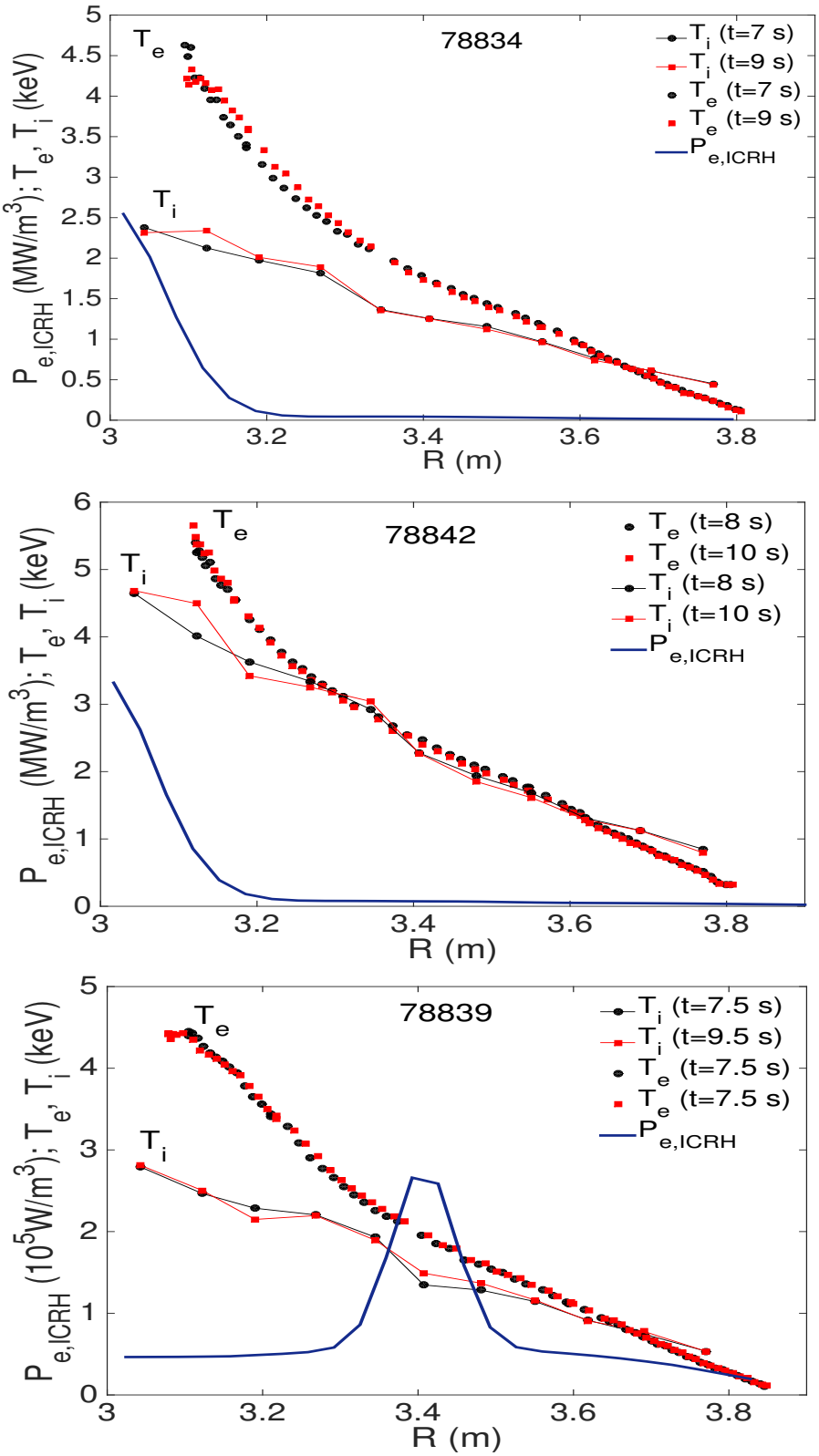

Figure 1: *Radial profiles of electron and ion temperatures and of P_{ICRH} deposition of discharges n. 78834 (ICRH on-axis, no NBI), n. 78842 (ICRH on-axis, 7 MW NBI) and n. 78839 (ICRH off-axis, no NBI) at two different times.*

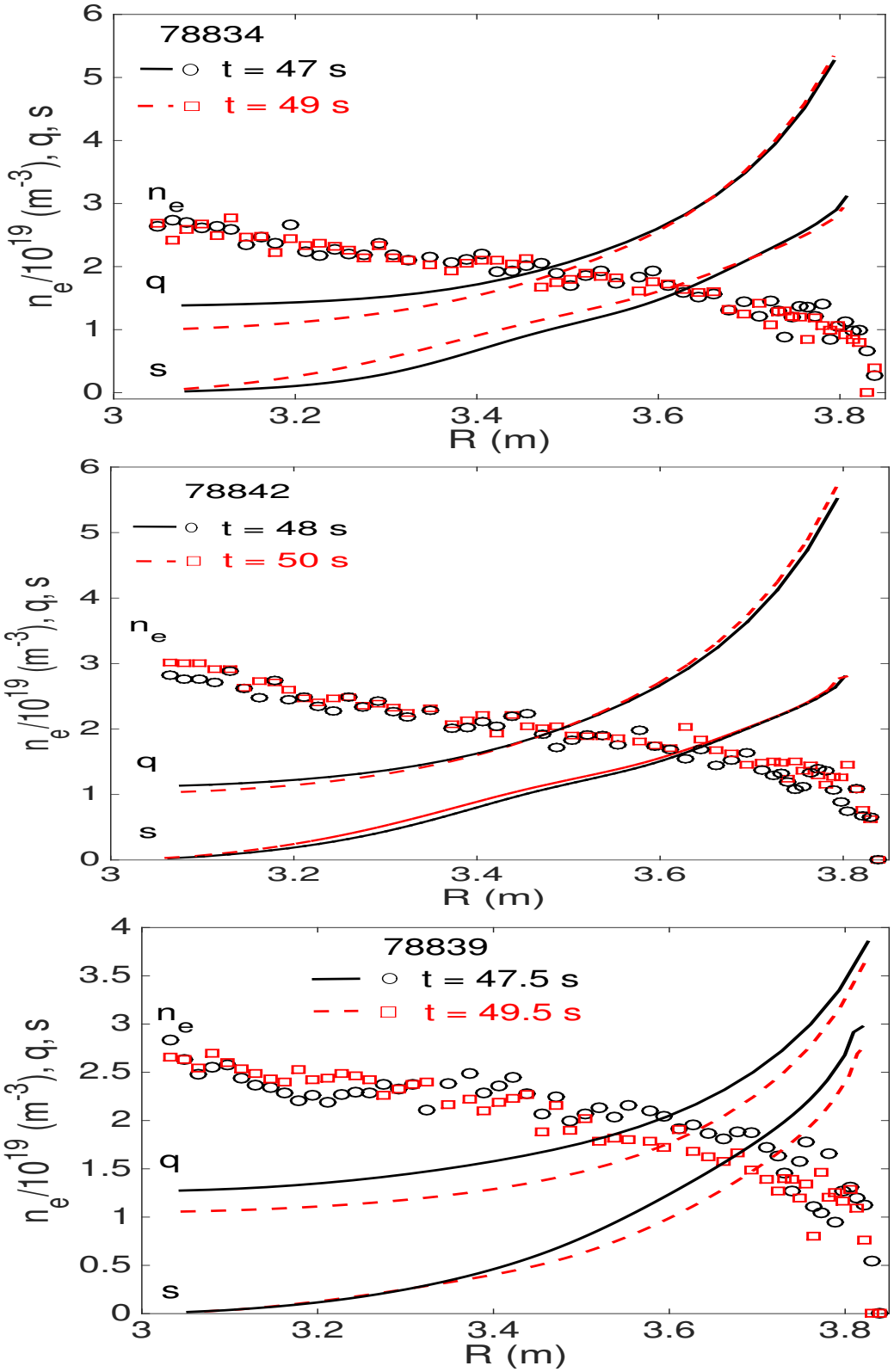

Figure 2: *Radial profiles of electron density, safety factor and magnetic shear of discharges n. 78834 (ICRH on-axis, no NBI), n. 78842 (ICRH on-axis, 7 MW NBI) and n. 78839 (ICRH off-axis, no NBI) at two different times.*

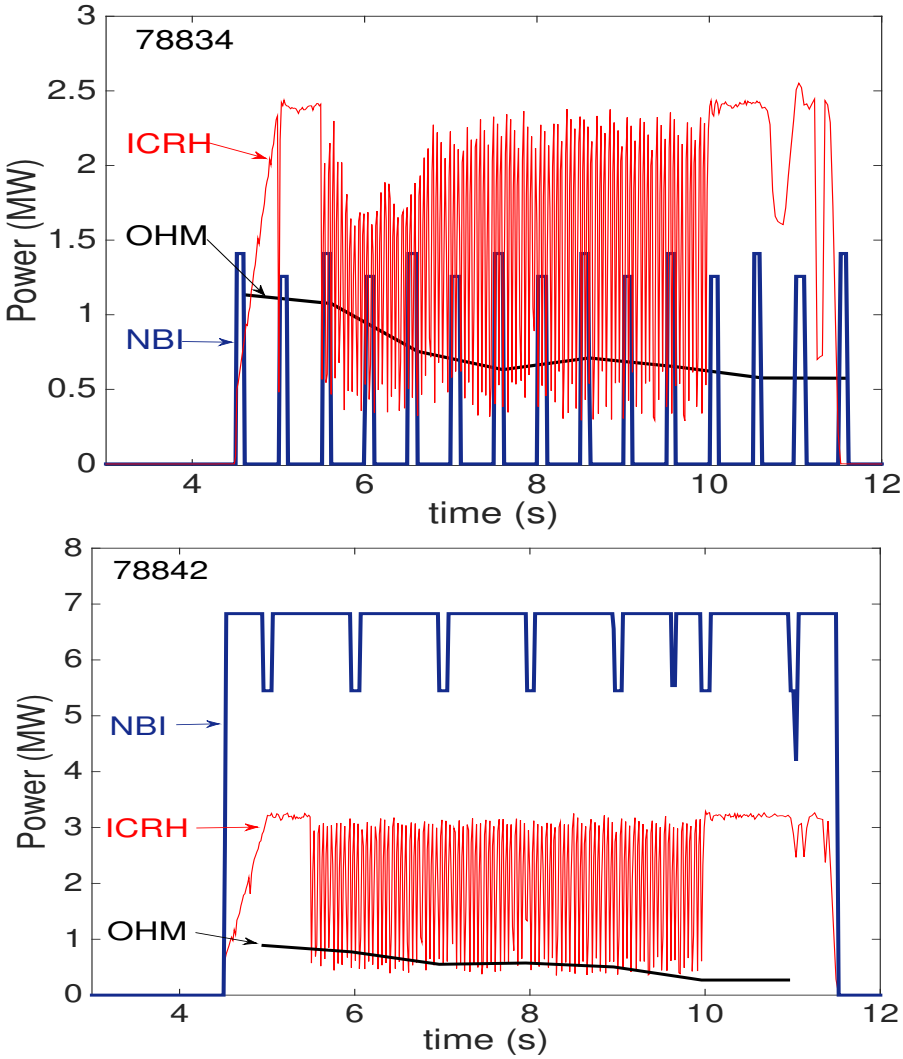

Figure 3: *Time waveforms of heating powers of discharges n. 78834 (ICRH on-axis, no NBI) and n. 78842 (ICRH on-axis, 7 MW NBI).*

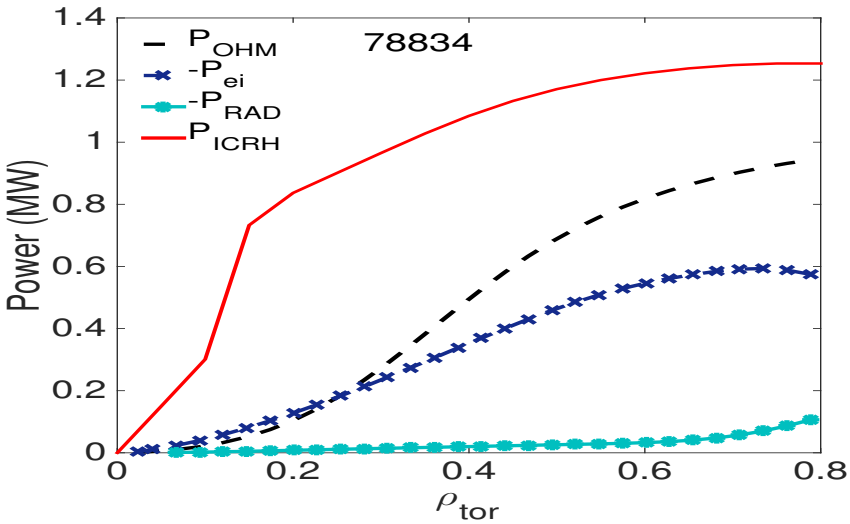

Figure 4: *Radial profiles of NBI heating (P_{NBI}), ohmic heating (P_{OHM}), ICRH heating (P_{ICRH}), radiated power (P_{RAD}) and heat exchange power due to ion-electron collisions ($P_{e,i}$) of the discharge n. 78834.*

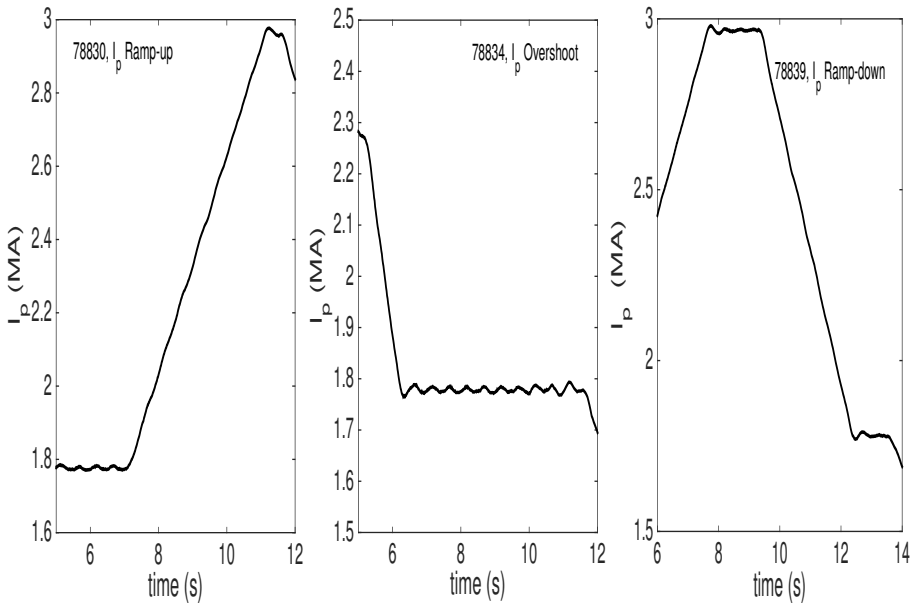

Figura 5: *Time waveforms of plasma current of discharges n. 78830 (I_p ramp-up), n. 78834 (I_p overshoot) and n. 78839 (I_p ramp-down).*

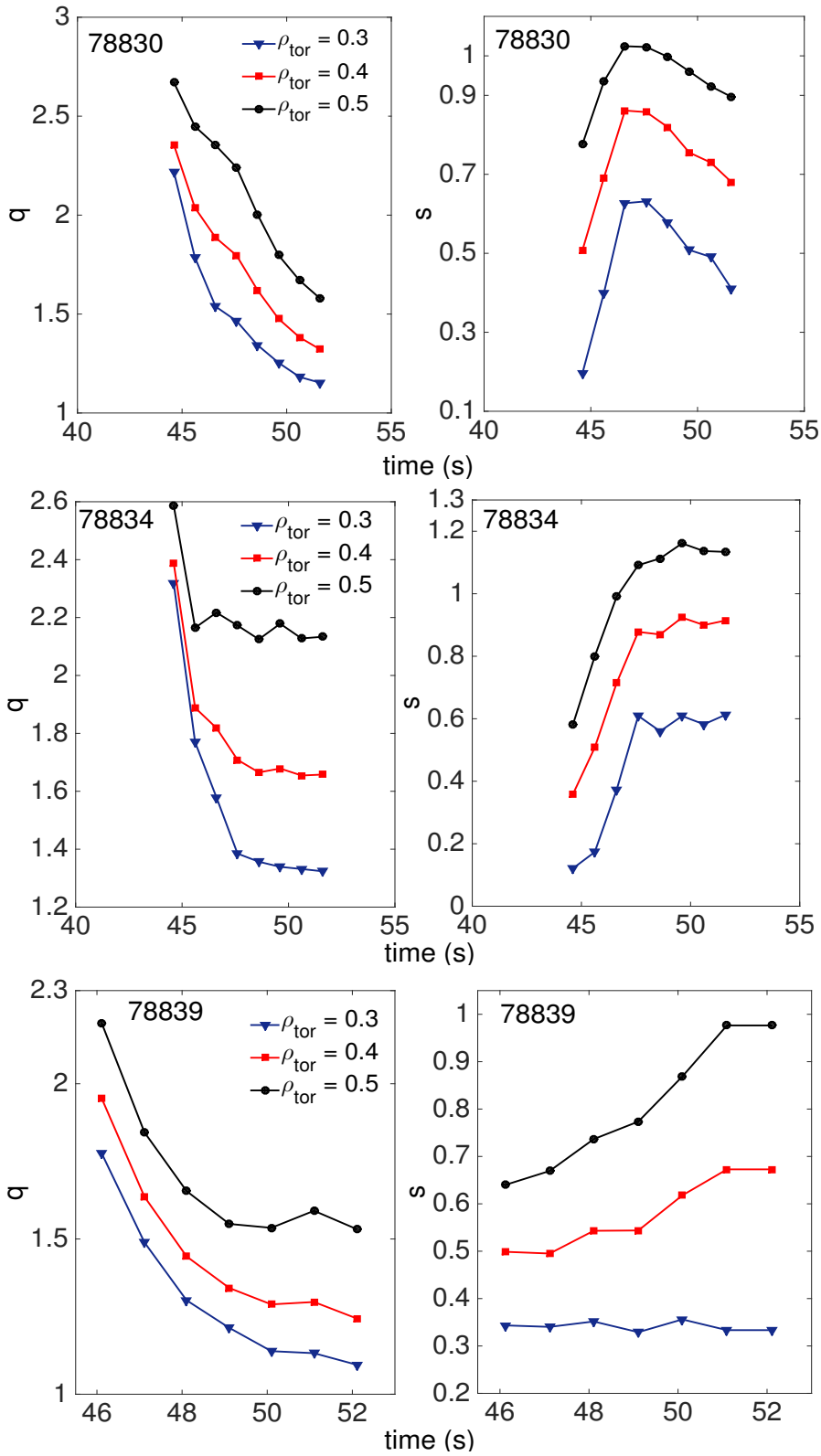

Figura 6: *Time evolution of safety factor and magnetic shear of discharges n. 78830 (I_p ramp-up), n. 78834 (I_p overshoot) and n. 78839 (I_p ramp-down) at* $\rho_{tor} = 0.33, 0.4, 0.5$.

ρ_{tor}	# fit	R/L_n	q	$\hat{s}$	T_e/T_i	ν_{eff}
$\rho_{tor} = 0.33$	(1)	1.7	1.3	0.3	1.4	0.2
	(2)	2.3	1.3	0.6	1.3	0.2
$\rho_{tor} = 0.4$	(1)	2.5	1.6	0.7	1.3	0.4
	(2)	2.6	1.5	0.8	1.3	0.4
	(3)	3.2	1.2	0.7	1.4	0.3
$\rho_{tor} = 0.5$	(1)	2.5	1.6	0.7	1.3	0.4
	(2)	2.7	2.3	0.9	1.3	0.4
	(3)	3.1	1.4	1	1.3	0.6
	(4)	2.6	2	1.2	1.2	0.6

Table 2: *Mean values of $s, q, R/L_n, T_e/T_i, \nu_{eff}$ of the data points used for the fits shown in Figure 7.*

where q_e^{res} is the residual flux not carried by TEMs (neglected in our case for the discharges with dominant electron heating), κ_c is the critical R/L_{Te}value, χ_s is the stiffness coefficient and $\theta(\bullet)$ is the Heaviside function. Equation (1) is a semi-empirical model called critical gradient model (CGM). Evaluating the values of q_e from the volume integral of the calculated sources at different radii and times, we can build the curve of the gyro-Bohm normalized flux $q_e^{GB}/q^{1.5}$ versus R/L_{Te} (where $q_e^{GB} = q_e/(n_e T_e^2 \rho_s/eBR^2)$), which allows to identify κ_c as the intercept to zero flux, whilst χ_s can be inferred from the slope of the curve. In this section only the results obtained from discharges with dominant electron heating in which TEM modes are dominant are shown. The results obtained from the heat flux scan are shown in Figure 7, where points with the same color and marks correspond to experimental data with same values of $s, q, R/L_n, T_e/T_i, \nu_{eff}$ (reported in Table 2). For each set of points the threshold and stiffness values have been evaluated with equation (1).

The threshold values are different at different radii and for different plasma parameters and in the following we will investigate by multilinear regressions to which parameters the threshold variations seen in Figure 7 are due. The values of stiffness and threshold are different at different radii. The stiffness is found to be higher at outer radius: the mean value of stiffness at $\rho_{tor} = 0.3$ is $\chi_s^{0.3} \approx 1.5$, at $\rho_{tor} = 0.4$ is $\chi_s^{0.4} \approx 3.2$ and at $\rho_{tor} = 0.5$ is $\chi_s^{0.5} \approx 3.2$.

The values of TEM threshold and stiffness are also calculated from the modulation data using the transport code ASTRA to simulate the profiles of time averaged T_e, amplitudes and phases with equation (1) as transport model and adjusting χ_s and κ_c to best fit the data. Using information from upper harmonics also the RF power deposition profile is reconstructed.The values found with this method are comparable with those obtained with the heat flux study and are shown in Figure 8 and in Figure 9 together with the fits obtained for T_e and $1st$ harmonic A, φ. The comparison with the values found with the heat flux scan is shown in Figure 10. Furthermore, the perturbative study confirms the growth of the stiffness with radius. In order to reproduce the profiles of the electron temperature with ASTRA simulations, a heat pinch $U \sim 3$ m/s is needed because of the high stiffness in the core indicated by the modulation profiles. An electron heat pinch was also observed in DIII-D, FTU, ASDEX-Upgrade and Tore Supra discharges [18, 19, 20, 21].

Since the subset of points with identical parameters plotted in Figure 7 is significantly smaller than the total set of points, in order to best estimate the correlations between TEM threshold and plasma parameters from the heat flux scan data, a multilinear regression method with the whole data set is used. In order to use values of κ_c instead of actual R/L_{Te} in the regressions, for each experimental measurement at a given radius and time, formula (1) is used with $q^{res} = 0$ and the mean values of stiffness found experimentally to extrapolate to the threshold from the experimental value of R/L_{Te}.

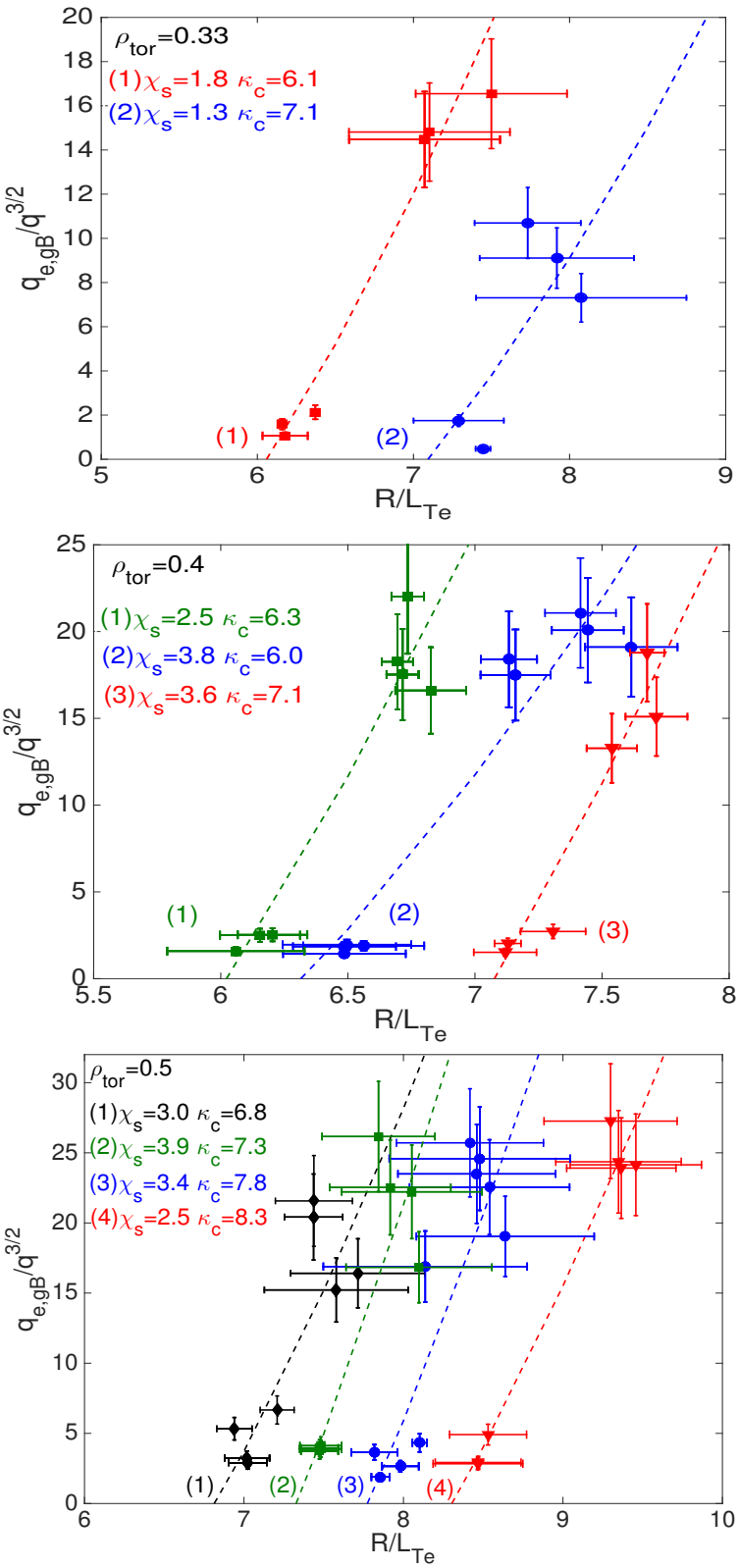

Figure 7: *Normalized electron heat flux as a function of R/L_{Te}at $\rho_{tor} = 0.3, 0.4, 0.5$. At each radius points with same colors and marks correspond to experimental points with same values of $R/L_n, s, q, T_e/T_i, \nu_{eff}$. For each set of points the corresponding value of χ_s is indicated. The threshold is the intercept at zero flux as indicate in the top figure.*

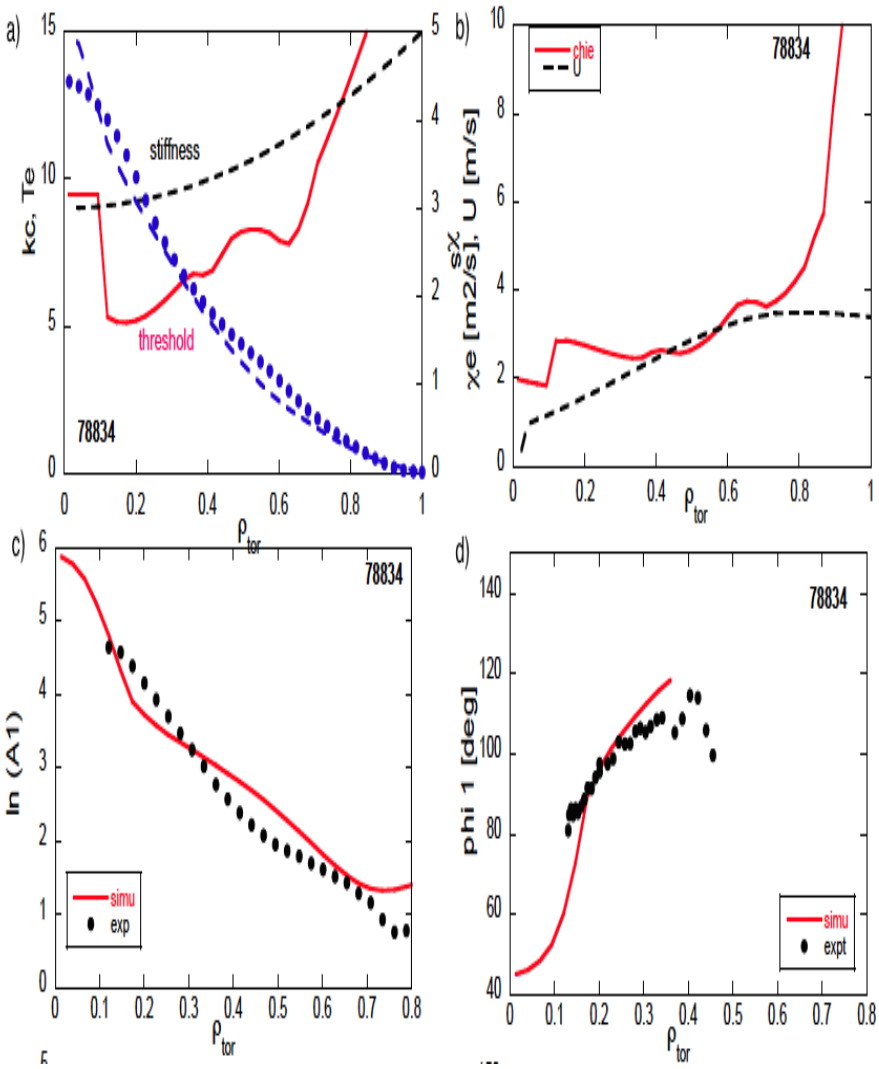

Figure 8: *ASTRA simulations of the T_e modulation for shot n. 78834 (ICRH on-axis). a)Profiles of T_e (blue points are the experimental values while blue dashed line is the profile obtained from the transport simulation), χ_s (black dashed line) and κ_c (red line). b)Profiles of χ_e (red line) and of the heat pinch$U$ (black dashed line). c) Profiles of $ln(A)$ of $1st$ harmonic (black points are the experimental values while red lines are the profile obtained from the transport simulations). d) Profiles ofϕ of $1st$ harmonic (black points are the experimental values while red lines are the profile obtained from the transport simulations).*

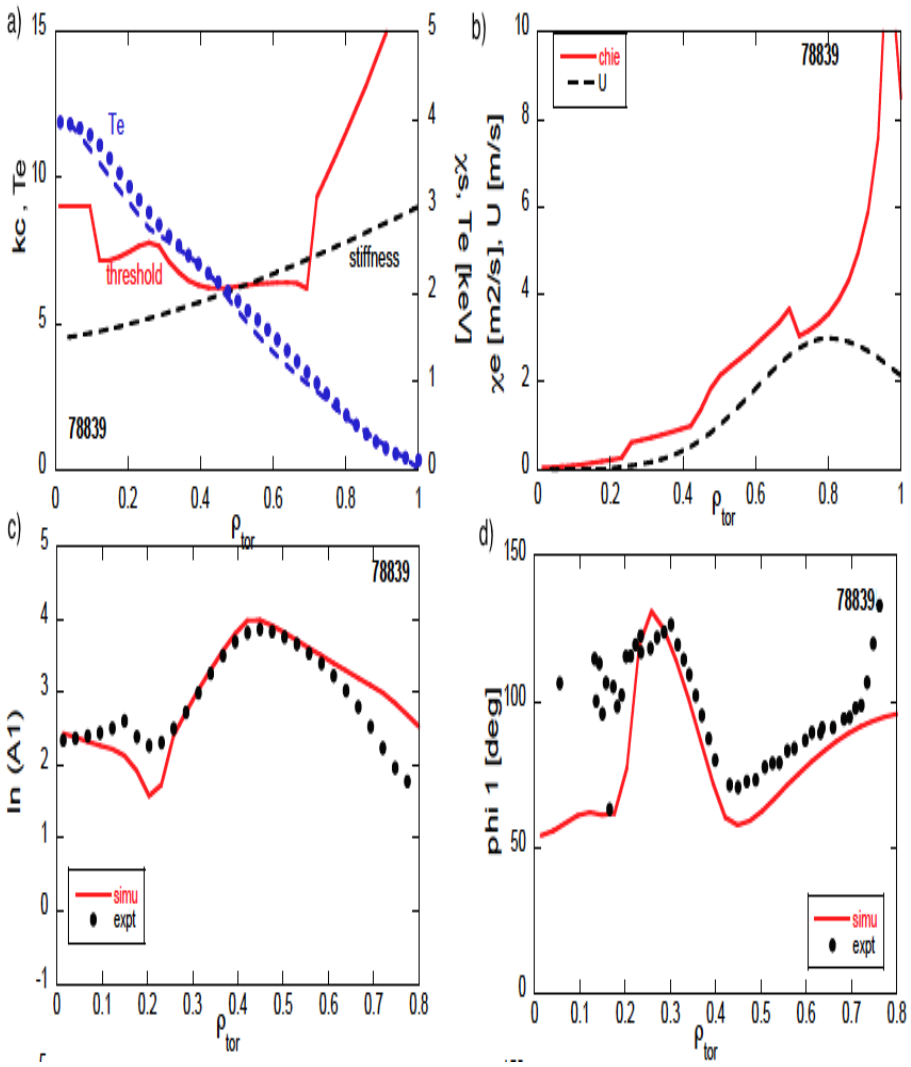

Figure 9: *ASTRA simulations of the T_e modulation for shot n. 78839 (ICRH off-axis). a)Profiles of T_e (blue points are the experimental values while blue dashed line is the profile obtained from the transport simulation), χ_s (black dashed line) and κ_c (red line). b)Profiles of χ_e (red line) and of the heat pinch$U$ (black dashed line). c) Profiles of $ln(A)$ of $1st$ harmonic (black points are the experimental values while red lines are the profile obtained from the transport simulations). d) Profiles ofϕ of $1st$ harmonic (black points are the experimental values while red lines are the profile obtained from the transport simulations).*

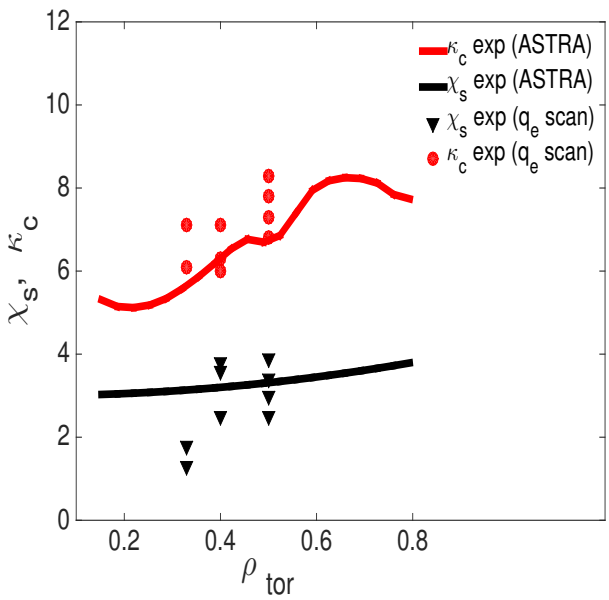

Figure 10: *Comparison between the values of stiffness and thresholds found with the heat flux scan and with the perturbative study.*

	κ_c	R/L_n	q	$\hat{s}$	ν_{eff}	T_e/T_i
κ_c	1	0.4	0.1	0.7	0.6	- 0.2
R/L_n	0.4	1	- 0.4	0.5	-0.1	0.2
q	0.1	- 0.4	1	0.04	0.5	- 0.2
$\hat{s}$	0.7	0.5	0.04	1	0.6	- 0.2
ν_{eff}	0.6	-0.1	0.5	0.6	1	- 0.4
T_e/T_i	- 0.2	0.2	- 0.2	- 0.2	- 0.4	1

Table 3: *Covariance matrix between the plasma parameters for the data at* $\rho_{tor} = 0.4, 0.5$.

The multilinear regressions express κ_c in the form $\kappa_c = \sum_j C_j X_j$, where C_j are the estimated regression coefficients and the vectors of regression variables X_j represent the considered plasma parameters. All values of κ_c used in the regressions are divided by the factor $(0.357\sqrt{\epsilon} + 0.271)/\sqrt{\epsilon}$, where $\epsilon = r/R$ and which takes into account the radius at which the thresholds are measured and allows regressions mixing data from different radii. This coefficient is the same used in [5]. In the present work, all the regressions are performed with a robust fit algorithm (Tukey algorithm), which uses iteratively re-weighted least squares with the bi-square weighting function, and are performed with MATLAB[1]. The strongest correlations found were those between κ_c and $R/L_n, \hat{s}, \nu_{eff}$. The covariance matrix for the considered parameters is shown in Table 3, it was calculated with MATLAB using all the experimental values at $\rho_{tor} = 0.4, 0.5$.

Looking at the covariance matrix and using multilinear regressions, weak correlations between κ_c and $q, T_e/T_i$ were found and these two parameters are not considered in the final regressions presented in the following. Since significant correlations were found also between the plasma parameters considered in the regressions $(\hat{s}, \nu_{eff}, R/L_n)$, in order to isolate the dependence on $\hat{s}$, a subset of data was identified at $\rho_{tor} = 0.4, 0.5$ in which ν_{eff} and R/L_n have a much lower relative variation compared to $\hat{s}$ $(0.4 \lesssim \nu_{eff} \lesssim 0.6, 2.2 \lesssim R/L_n \lesssim 3.2, 0.4 \lesssim \hat{s} \lesssim 1.31)$. This allowed us to calculate the correlation

[1] http://www.mathworks.it/

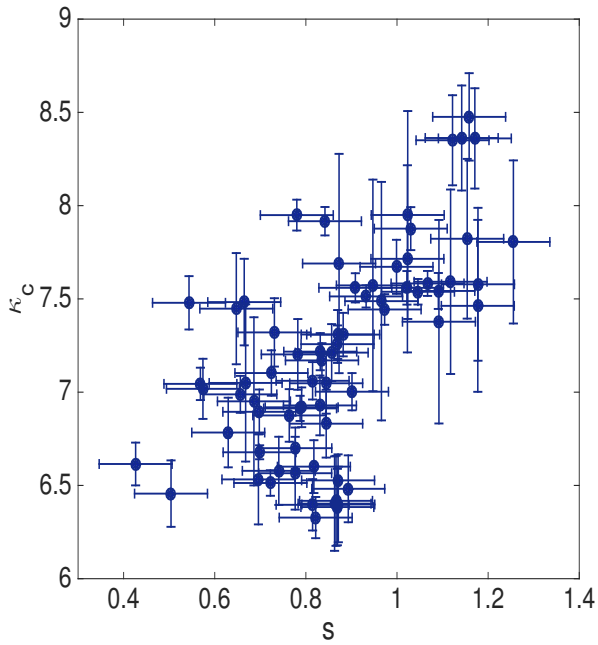

Figure 11: *Critical thresholds κ_c as a function of magnetic shear s for the experimental data at $\rho_{tor} = 0.4, 0.5$ with $0.4 \lesssim \nu_{eff} \lesssim 0.6, 2.2 \lesssim R/L_n \lesssim 3.2$.*

between κ_c on $\hat{s}$:

$$\kappa_c \approx \frac{0.357\sqrt{\epsilon} + 0.271}{\sqrt{\epsilon}} \left((5.5 \pm 0.4) + (2.4 \pm 0.4)\hat{s}\right). \tag{2}$$

In Figure 11 the values of κ_c versus $\hat{s}$ of the sub dataset used for the regression (2) are shown; the figure and the multilinear regression results indicate a positive correlation between TEM threshold and the magnetic shear. This could be a the first experimental confirmation of the direct effect of $\hat{s}$ on the TEM threshold predicted by theory [5].

Fixing the value of the coefficient of $\hat{s}$ to 2.5 an estimate of the coefficients of R/L_n and ν_{eff} was found by regression over the whole dataset:

$$\kappa_c^{Reg} \approx \frac{0.357\sqrt{\epsilon} + 0.271}{\sqrt{\epsilon}} \left((1.7 \pm 0.5) + (0.3 \pm 0.1)\frac{R}{L_n} + 2.5\hat{s} + (1 \pm 0.2)log(1 + 20\nu_{eff})\right). \tag{3}$$

Formula (3) is only indicative. For our range of plasma parameters, the positive correlation between κ_c and ν_{eff} was expected by linear gyrokinetic simulation and from previous experimental work on AUG [7]. In the present dataset the evidence is less clear but still inside uncertainties. The positive correlation between κ_c and R/L_n is opposite to the one predicted by gyrokinetic theory and is likely due to the strong correlation between R/L_n and $\hat{s}$ associated to a curvature pinch [22, 23, 24]. In other words, the dependence of κ_c on R/L_n cannot be isolated within this dataset.

3 Modelling and comparison with experiments

A set of linear and nonlinear simulations with the gyrokinetic code GKW [25, 26] were carried out on supercomputers HECTOR[2] and HELIOS[3] in order to study the effects of a number of plasma parameters on TEMs. With the results obtained with the linear simulations an indicative formula to predict TEMs thresholds was found. In this section the values of thresholds predicted by this formula are compared both with the experimental values and with the values predicted by a previous formula presented by A. G. Peeters in [5]:

$$\kappa_c^{[5]} \approx \frac{0.357\sqrt{\epsilon}+0.271}{\sqrt{\epsilon}}\left(4.90 - 1.21\frac{R}{L_n} + 2.68\hat{s} + log(1+20\nu_{eff})\right) \tag{4}$$

This formula was derived from linear simulations with the code GS2, using plasma parameters from discharges of ASDEX-Upgrade and circular geometry and was not meant to give an universal scaling but rather to highlight the main dependences of TEM threshold on plasma parameters in the range of the AUG discharges considered.

3.1 Linear simulations

In a linear simulation, GKW finds the fastest growing eigenmode in the plasma excited by a perturbation of a prescribed length scale. This length scale is defined by a bi-normal (perpendicular to both the magnetic field line and the flux surface normal vector) Fourier mode wavenumber k_θ that is provided as input to the code. The main output of the code used in this analysis is the linear growth rate of the eigenmode, and rom its other characteristics, such as real frequency or parallel structure, the main driving mechanism of the instability can be determined ((ITG, TEM etc.).

All linear simulations have been performed with kinetic electrons, collisions, Miller geometry, electro-static perturbations only ($\beta = 0$) and $k_\theta\rho_i = 0.4$. The plasma parameters used as inputs in the simulations are typical values of the TEM session discharges at $\rho_{tor} = 0.5$. The reference set is given by electron and ion density $n_e = n_i = 1.97 \cdot 10^{19}$ m^{-3}, electron temperature $T_e = 1.45$ keV, ion temperature $T_i = 1.15$ keV, normalized inverse gradient lengths of the density and ion temperature profile are $R/L_n = 3.4, R/L_{Ti} = 4$, safety factor $q = 2.01$, magnetic shear $\hat{s} = 0.99$, inverse aspect ratio $\epsilon = r/R = 0.19$, and effective charge $Z_{eff} = 2.16$. Starting from the reference case, the values of the growth rate as a function of R/L_{Te} are calculated in the range $0 \leq R/L_{Te} \leq 16$, with different values of $s, R/L_n, \nu_{eff}, T_e/T_i$ to study the correlations between these parameters and TEM growth rate. The values of the threshold are then obtained by performing a parabolic fit on the points of the curve of γ versus R/L_{Te} where TEM modes are dominant (real part of the frequency $\omega_{k_\theta} < 0$) and then by an extrapolation to $\gamma = 0$.

Figure 12 shows results obtained for the scans in $\hat{s}, R/L_n, \nu_{eff}$ and T_e/T_i. The linear simulations indicate a stabilizing effect of the magnetic shear $\hat{s}$ and of the collisionality while a destabilizing effect of R/L_n on TEM is predicted, especially for higher values of R/L_n ($R/L_n > 3$). The effect of T_e/T_i, while significant in the ITG regime, is very weak in the TEM regime.

An indicative formula for the TEM threshold is obtained using the results from linear simulations:

$$\kappa_c^{GKW} \approx \frac{0.357\sqrt{\epsilon}+0.271}{\sqrt{\epsilon}}\left(-1.2 - 0.11\frac{R}{L_n} + 2.5\hat{s} + 2.5log(1+20\nu_{eff})\right). \tag{5}$$

[2] http://www.hector.ac.uk/
[3] http://www.iferc.org/

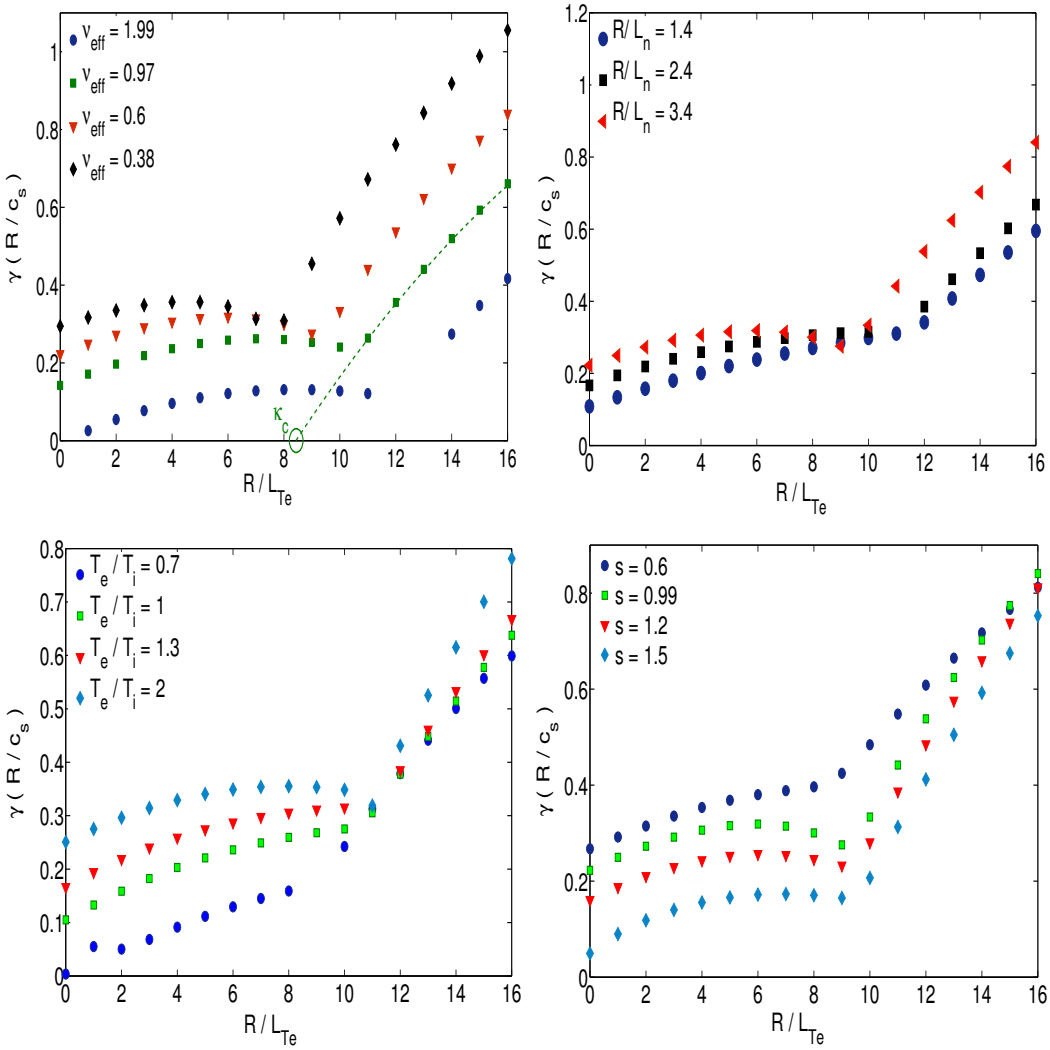

Figure 12: *Normalized linear growth rates as a function of R/L_{Te} obtained with linear gyrokinetic simulations with GKW. The values of thresholds are obtained with quadratic fits on the points where the most unstable modes are the TEM as shown in the first figure.*

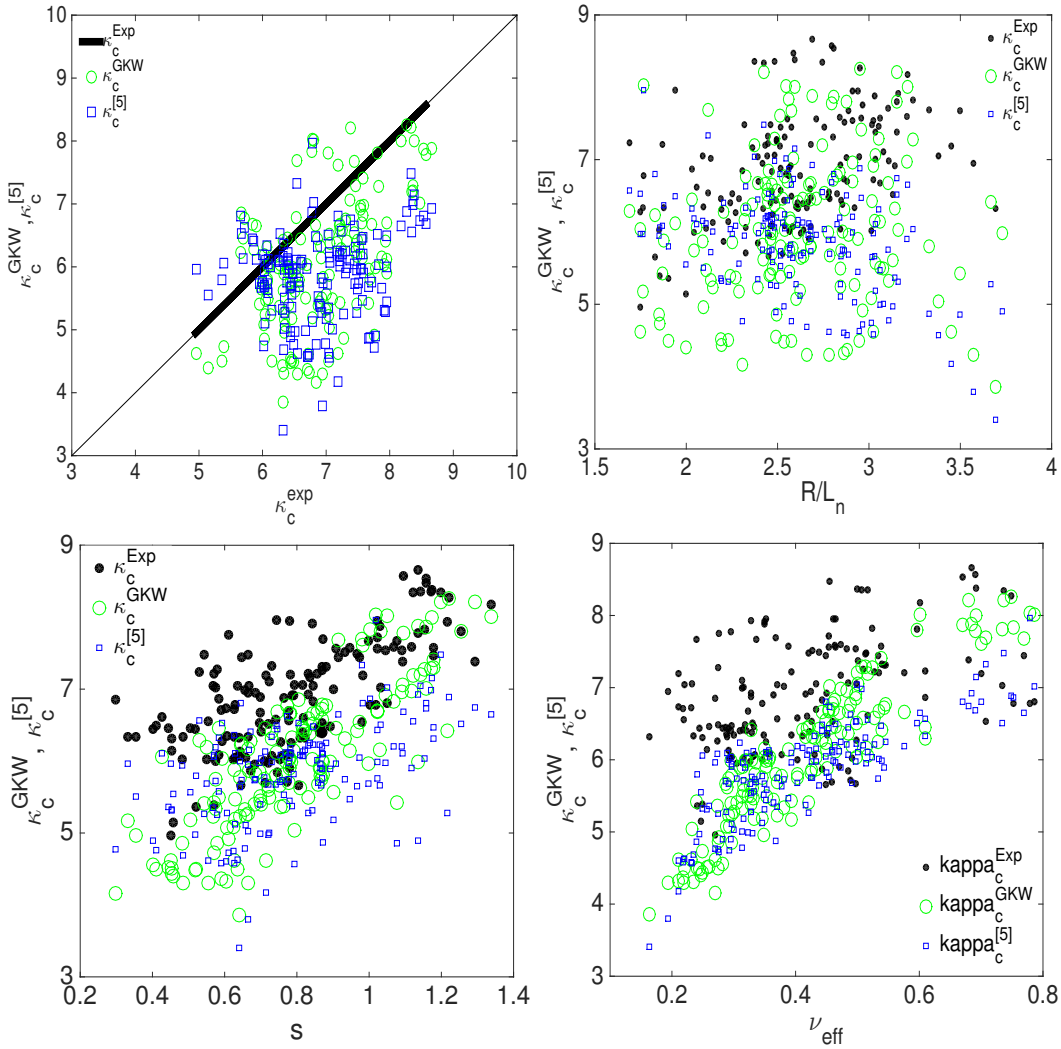

Figure 13: *Experimental values of κ_c(black circles), values of κ_c^{GKW} (green circles) obtained with (5) using experimental values of $R/L_n, s, \nu_{eff}$ and values of $\kappa_c^{[5]}$ (blue squares) obtained with (4) using experimental values of $R/L_n, s, \nu_{eff}$ as a function of $\kappa_c^{exp}, R/L_n, s$ and ν_{eff}.*

The comparisons with the experimental thresholds and with the ones obtained with formula (4) are shown in Figure 13. First of all, the trend of the thresholds obtained with the formula based on GKW linear simulations is in good agreement with the experimental ones. The simulations predict the stabilizing effect of the magnetic shear, also found experimentally, and the weak effect of R/L_n (weaker than that found in [5] for their range of parameters). The stabilizing effect of collisionality predicted by the simulations is stronger than that found experimentally.s The correlation between ν_{eff} and $\hat{s}$ found in the experimental data could hide a stronger experimental correlation between κ_c and ν_{eff}. The values of the thresholds predicted by linear simulations are in good quantitative agreement with the experimental ones.

3.2 Nonlinear simulations

Non-linear gyrokinetic simulations allow to calculate the electron heat flux values and so to do a direct comparison with the experimental electron temperature stiffness. In a non-linear run the simulation domain and spatial resolution in the perpendicular plane is determined by a set of coupled bi-normal and radial Fourier-modes. Input to the code are the range and number of bi-normal modes and number of radial modes. The coupling between these modes provides a numerical scheme which is equivalent to the ballooning approximation commonly applied in other gyrokinetic codes, such as GS2.

In all simulations the value of the maximum binormal mode is fixed to $(k_\theta \rho_i)_{max} = 1.6$, collisions are considered, Miller geometry is used and all simulations have $\beta = 0.0008$ (to stabilize some long wavelength instabilities, like the electrostatic shear-Alfven waves, allowing a much larger stable time step). The plasma parameters used as inputs are taken at $\rho_{tor} = 0.5$ from the pulse n.78834 and averaged in the time interval $6.855 \leq t \leq 7.155$ s. The main input parameters are electron and ion density $n_e = n_i = 1.94 \cdot 10^{19}$ m^{-3}, electron temperature $T_e = 1.35$ keV, ion temperature $T_i = 1.11$ keV, normalized inverse gradient lengths of the density and ion temperature profile $R/L_n = 2.63, R/L_{Ti} = 3$, safety factor $q = 2.08$, magnetic shear $\hat{s} = 1.14$, inverse aspect ratio $\epsilon = r/R = 0.19$, and effective charge $Z_{eff} = 2.16$. The values of the heat flux at $\rho_{tor} = 0.5$ are calculated for $R/L_{Te} = 8.5, 9.1, 9.5, 10.1, 10.5$. All simulations were carried out considering 43 values of binormal modes k_θ and 167 values of radial modes k_Ψ. An estimate of threshold and stiffness is obtained performing a parabolic fit on the curve $q_{e,gB}/q^{3/2}$ versus R/L_{Te} following the formula (1). The obtained results are shown in Figure 14. Considering the uncertainties on the measurements of the plasma parameters used as input for the simulations and the uncertainty on the theoretical determination of the threshold values, the experimental threshold and the theoretical threshold are in good agreement. The flux levels and the related stiffness are lower than the experimental ones, but a rigorous study changing the input parameters in the experimental error bar range and considering high-k ETG modes, which may contribute to the transport, is needed to achieve an accurate comparison between simulations and experiments. This study is not included in this preliminary analysis due to limited computational resources, but will be presented in a future paper.

4 TEM studies in plasmas with significant ion heating

In discharges with significant ion heating (6.8 MW of NBI heating) lower values of R/L_{Te} were found, compared with discharges without NBI heating for same values of normalized heat flux $q_{e,gB}$, as shown in Figure 15.

The main differences in plasma parameters between these discharges and those with dominant electron heating are different values of T_e/T_i, different rotation of the plasma and different values of R/L_{Ti}. The effect of T_e/T_i, as indicated by the linear simulations with GKW, doesn't seem to be the cause of the observed decrease in R/L_{Te}.

High values of R/L_{Ti} could have some effects on the electron heat transport, if a significant fraction of electron heat flux is driven by ITG modes. However we know from [1, 2] that in this kind of shots with NBI and ICRH, strong ion de-stiffening is observed (ascribed to electromagnetic stabilization of ITG by fast ions pressure gradient), which leads to a significant decrease of flux driven by ITGs (both ion and electron flux). Therefore this mechanism does not appear a plausible candidate to explain observations.

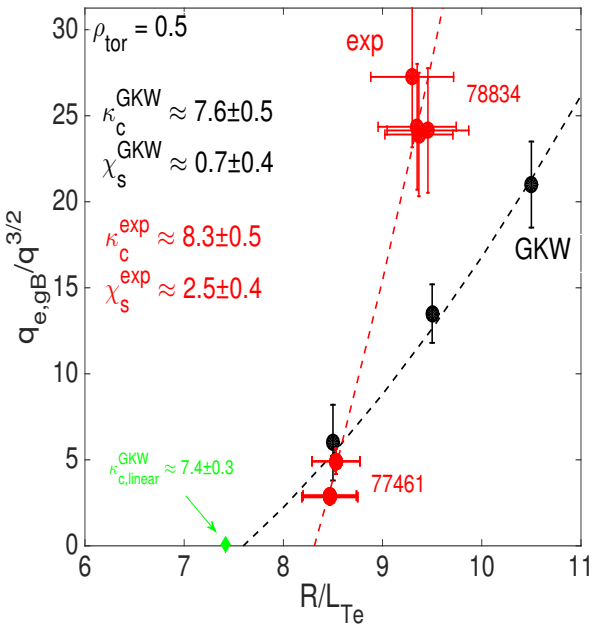

Figure 14: *Electron heat fluxes obtained with nonlinear gyrokinetic simulations with GKW. Red squares indicate the experimental data, black circles indicate the fluxes obtained from nonlinear gyrokinetic simulations and the green diamond indicates the thresholds obtained from linear gyrokinetic simulations with GKW.*

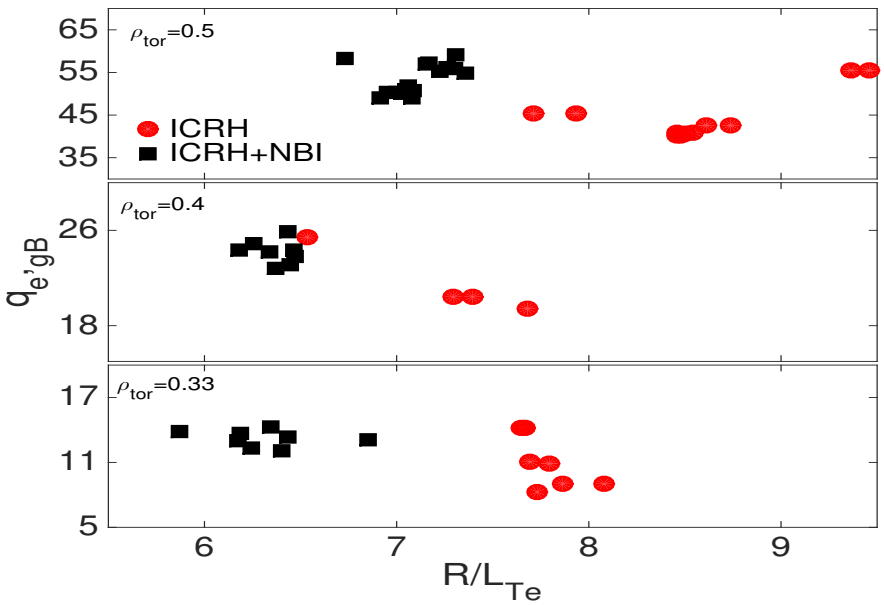

Figure 15: *Experimental values of R/L_{Te} at same value of $q_{e,gB}$ in function of $q_{e,gB}/q_{i,gB}$ at $\rho_{tor} = 0.3, 0.4, 0.5$. Red circles are data points from discharges without NBI heating while black squares are data points from discharges with NBI heating.*

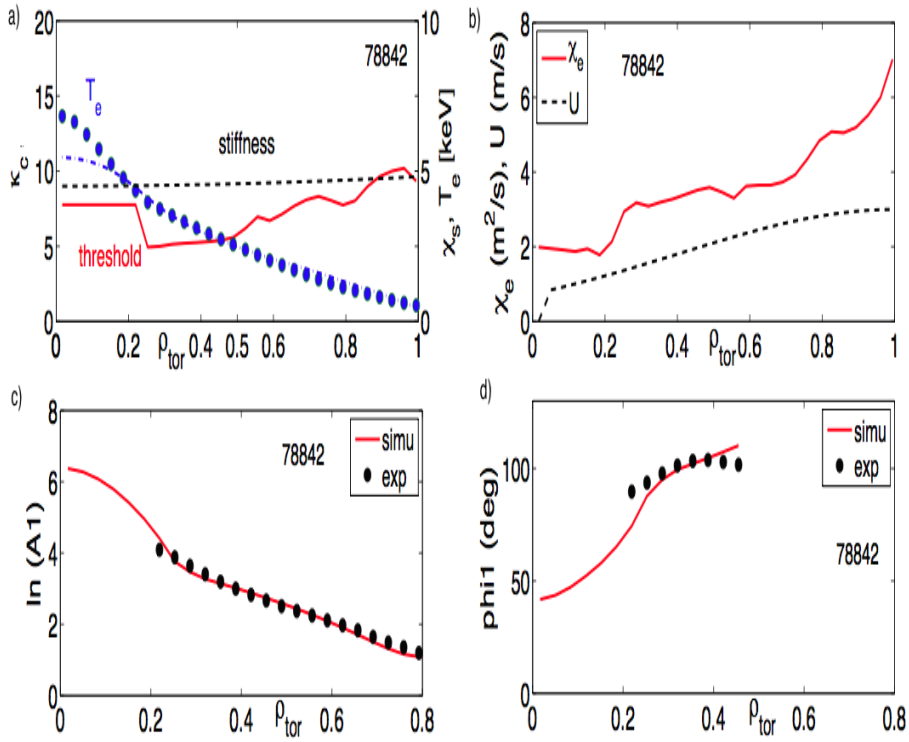

Figure 16: *ASTRA simulations of the T_e modulation for shot n. 78842 (ICRH on-axis, NBI=7 MW). a)Profiles of T_e (blue points are the experimental values while blue dashed line is the profile obtained from the transport simulation), χ_s (black dashed line) and κ_c (red line). b)Profiles of χ_e (red line) and of the heat pinch$U$ (black dashed line). c) Profiles of $ln(A)$ of 1st harmonic (black points are the experimental values while red lines are the profile obtained from the transport simulations). d) Profiles ofϕ of 1st harmonic (black points are the experimental values while red lines are the profile obtained from the transport simulations).*

A second effect that could be correlated to high value of R/L_{Ti} could concern the electron stiffness. The perturbative study, shown in Figure 16, indicates indeed higher values of stiffness with NBI heating. An increase of electron stiffness in presence of NBI heating has also been previously reported [9, 10, 11]. However, the effects of the presence of NBI heating on ITG and the results from linear simulations with GKW, shown in Figure 17, indicate that the higher electron stiffness are not correlated with the higher values of R/L_{Ti}. Higher values of R/L_{Ti}, as indicate in Figure 17, seem to stabilize the TEM for lower values of $k_\theta \rho_i$, which are known to be the responsible of most of the heat flux due to TEM.

A third possibility is that, due to lower values of T_e/T_i, ETG modes could be more unstable [30] and increase the electron heat transport.

We would like to underline the opposite behavior observed in the ion and electron channels when NBI heating is added to pure ICRH plasma. This is shown in Figure 18. For ions, as reported in [1, 2], a significant reduction in stiffness is observed. Unfortunately, this is not observed in the electron channel, for which at the contrary an increase in stiffness and a threshold reduction are observed. Since ITER will be dominated by electron heating, i.e. $T_i \leqslant T_e$, it is important to continue the effort to understand the mechanisms that govern electron transport in mixed ITG+TEM regime, since such high electron stiffness (if it would be extrapolated to ITER) may partly cancel the benefit of ion de-stiffening. On the positive side, we note that a beneficial point is in any case that the TEM electron

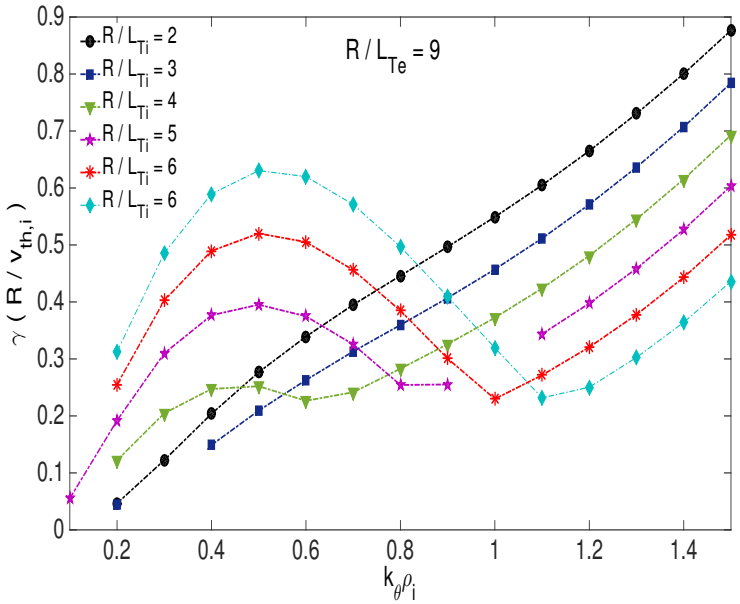

Figure 17: *Linear growth rates vs $k_\theta \rho_i$ for different values of R/L_{Ti} obtained from linear simulations with GKW.*

threshold is significantly higher than the ITG ion threshold, therefore allowing some increase in R/L_{Ti} due to de-stiffening even in presence of high electron stiffness.

5 Conclusions

Experiments have been carried out in JET L-mode plasmas with dominant ICRH electron heating to explore the q and $\hat{s}$ dependence of TEMs using I_p ramp-up, ramp-down and overshoots in order to obtain non correlated variations of the safety factor and magnetic shear. Scans of electron heat flux and T_e modulation have been used to determine electron threshold and stiffness. The experimental results have been found in good agreement with theoretical predictions, in particular a first experimental confirmation of the stabilizing effect of the magnetic shear $\hat{s}$ on TEMs has been obtained. Also the predicted effect of ν_{eff} on TEMs was observed experimentally while no experimental evidence of strong dependences of the TEM threshold on q and T_e/T_i was found. The effect of R/L_n, given the high correlation of this parameter with $\hat{s}$, was not isolated in a satisfactory manner, but it seems to be weaker than the effect of other parameters. Furthermore, an increase of the experimental electron stiffness with radius was observed. To be noted, a convective component of the electron heat flux was required in the simulations to achieve good reproduction of the data.

With the experimental parameters as input, a large number of linear gyrokinetic simulations and also a limited number of non-linear simulations were carried out using GKW. The simulations have confirmed the stabilizing effect of magnetic shear and collisionality and predict a weak destabilizing effect of R/L_n. The study of the effect of T_e/T_i suggests that this parameter does not significantly affect either the values of the threshold or the growth rate of the TEMs. An indicative formula for the prediction of the TEM threshold was obtained from the results of the linear simulations. This is found to slightly underestimate the experimental observations. Nonlinear simulations with GKW has allowed a comparison with the experimental stiffness. In general, linear and nonlinear gyrokinetic

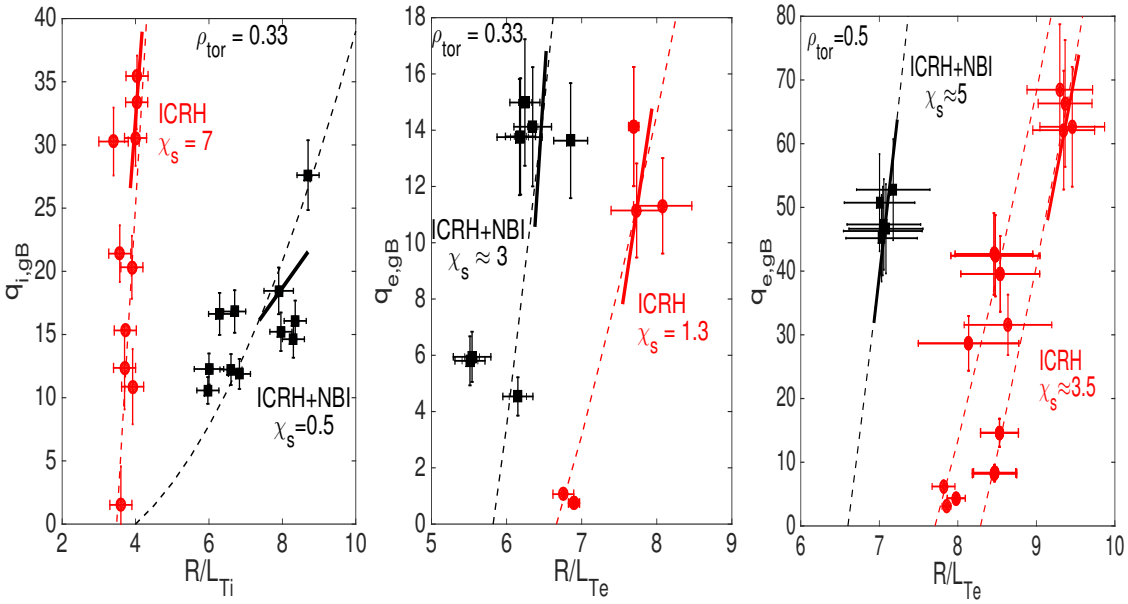

Figure 18: *$Q_{i,gB}$ vs R/L_{Ti} at $\rho_{tor} = 0.33$ from [1] and $Q_{e,gB}$ v R/L_{te} at $\rho_{tor} = 0.33, 05$ for similar plasmas without NBI heating (red circles) and with NBI heating (black squares). Dotted lines indicate the quadratic fits used for the identification of threshold and stiffness while continuos segments indicate the fits obtained from the modulation. While for ions the addition of NBI heating leads to an increase of R/L_{Ti} due to a significant reduction of ion stiffness, for electrons the addition of NBI has the opposite effect, decreasing R/L_{Te} due to both a threshold reduction and an increase in stiffness.*

simulations with GKW are in agreement with the experimental values of the TEM threshold and also with the observed dependences of the threshold on plasma parameters.

When significant ion heating (NBI heating) is added, leading to a transition from dominant TEM to mixed ITG-TEM with dominant ITG, a higher electron stiffness and lower values of R/L_{Te} with same levels of $q_{e,gB}$ are observed. These effects could be due to the presence of other modes like ETG (Electron Temperature Gradient modes) due to lower values of T_e/T_i. The full theoretical understanding, via nonlinear simulations, of electron heat transport in these mixed ITG-TEM conditions goes beyond the scope of the present paper, but it deserves further work both experimentally and theoretically given its importance to achieve reliable predictions for ITER, which is electron heating dominated.

Acknowledgement

The authors would like to thank Jonathan Citrin for precious advice and stimulating discussions.

A part of this work was carried out using the HELIOS supercomputer system at Computational Simulation Centre of International Fusion Energy Research Centre (IFERC-CSC), Aomori, Japan, under the Broader Approach collaboration between Euratom and Japan, implemented by Fusion for Energy and JAEA. The linear gyrokinetic simulations were performed on Hector supercomputer (UK Research Councils).

This work has been carried out within the framework of the EUROfusion Consortium and has received funding from the Euratom research and training programme 2014-2018 under grant agreement No 633053. The views and opinions expressed herein do not necessarily reflect those of the European

Commission.

References

[1] P. Mantica et al., Physical Review Letters 107, 135004 (2011)
[2] J. Citrin, Nuclear Fusion 54, 023008 (2014)
[3] J. Weiland, IOP Publishing Ltd, 2000
[4] W. Horton, Reviews of Modern Physics 71, 735 (1999)
[5] A. G. Peeters et al., Physics of Plasmas 12, 022505 (2005)
[6] M. Romanelli, G. Regnoli, C. Bourdelle, Physics of Plasmas 14, 082305 (2007)
[7] F. Ryter et al., Physical Review Letters 95, 085001 (2005)
[8] A. Casati, Physics of Plasmas 15, 042310 (2008)
[9] J. C. DeBoo et al., Physics of Plasmas 19, 082518 (2012)
[10] X. Garbet et al., Plasma Physics and Controlled Fusion 46, B557 (2004)
[11] P. Mantica, F. Ryter, EFDA_PR(06)07 (2007)
[12] D. Van Eester et al., Plasma Physics and Controlled Fusion 51, 044007 (2009)
[13] P. Mantica, F. Ryter, C. R. Physique 7, (2006)
[14] N. J. Lopes Cardozo, Plasma Physics and Controlled Fusion 37, 799 (1995)
[15] G. V. Pereverzev, P. N. Yushmanov, Max-Planck-Institute fur Plasmaphysik, (2002)
[16] G. Cenacchi and A. Taroni, Rapporto ENEA RT/TIB (88)5 (1998)
[17] F. Imbeaux, F. Ryter and X. Garbet, Plasma Physics and Controlled Fusion 43, 1503 (2001)
[18] P. Mantica et al., Plasma Physics and Controlled Fusion 48, 385 (2006)
[19] P. Mantica et al., Physical Review Letters 95, 185002 (2005)
[20] X. L. Zou et al., 35th EPS Conference on Plasma Physics , Hersonissos (2008)
[21] S. D. Song et al., Nuclear Fusion 52, 033006 (2012)
[22] M. B. Isichenko et al., Physics of Plasmas 3, 1916 (1996)
[23] X. Garbet et al., Physical Review Letters 91, 035001-1 (2003)
[24] C. Angioni et al., Plasma Physics and Controlled Fusion 51, 124017 (2009)
[25] A.G. Peeters et al., Computer Physics Communications, 180, 2650, (2009)
[26] A.G. Peeters, D. Strintzi, Phys. Plasmas 11, 3748, (2004)
[27] F. Ryter et al., Nuclear Fusion 51, 113016 (2011)
[28] S. C. Guo, F. Romanelli, Physics of Fluid B 5, 520 (1993)
[29] P. Mantica et al., 124033 (2011)
[30] F. Jenko, W. Dorland, G. W. Hammett, Physics of Plasmas 9, 4096 (2001)